Int J Adv Manuf Technol (2018) 94:4469–4478
DOI 10.1007/s00170-017-1150-z

ORIGINAL ARTICLE

Investigations into side gap in wire electrochemical micromachining (wire-ECMM)

Aakash Tyagi[1] · **Vyom Sharma**[1] · **V. K. Jain**[1,2] · **J Ramkumar**[1]

Received: 20 February 2017 / Accepted: 19 September 2017 / Published online: 5 October 2017

Abstract Electrochemical machining (ECM) process is now in application in various industries like maritime, automobile, and aerospace. Wire-ECM, a variant of ECM, is now under investigation, for its applications in electronics industries for the fabrication of PCB on conductive metals like copper and in medical industries for the fabrication of micro needles with textures on its surface for the painless delivery of drugs. One of the most important parameters in wire-ECM is side gap. This paper aims at obtaining minimum side gap for the given machining conditions. In order to achieve this, three different workpieces of Al, Cu, and stainless steel are examined. Effects of different electrolytes on the side gap are also examined. Later on, different electrolytes at different temperatures are used to study their effect on the side gap. Finally, optimum parameters are determined in order to keep the side gap to a minimum level. In order to keep the findings significant for industrial applications, machining rate is kept as high as 5 μm/s. Other relevant process parameters are so derived that the machining process can attain stability at high feed rate. To realize this, regulated DC power supply is used. Average side gap was finally reduced to 26.8 μm using a commercially available copper wire of diameter 90 μm.

Keywords Wire-ECMM · Side gap · Pourbaix diagram · Frontal gap · Passivation layer

✉ Aakash Tyagi
aakasht@iitk.ac.in

✉ Vyom Sharma
vyom@iitk.ac.in

V. K. Jain
vkjain@iitk.ac.in

J Ramkumar
jrkumar@iitk.ac.in

[1] Department of Mechanical Engineering, Indian Institute of Technology, Kanpur, India

[2] Present address: Department of Mechanical Engineering, M.A.N.I.T, Bhopal, India

1 Introduction

Ever increasing popularity and acceptance of the ECM process are owing to its advantages over other processes. Absence of heat-affected zone (HAZ) and recast layer has given this process an edge over other advanced machining processes (AMPs) like EDM, LBM, EBM, etc. Due to the nature of material removal in this process, ion by ion dissolution, the parent material properties are almost retained after performing this machining operation. However, good dimensional control of an electrochemically machined component is normally difficult to obtain, the design of the tool generally being a serious problem [1]. Research had been done on tool design mainly by boundary layer techniques and finite element analysis using derivations based on Laplace, Ohm, and Faradays' laws [2–4]. One particular variant of ECM is wire electrochemical machining (wire-ECM). Popularity of this process is increasing due to the fact that use of wire as a tool eliminates the need of heavy and automated tooling as well as the need of heavy power input.

Wire-ECM is under investigation by very few researchers around the globe. Jain and Pandey [5] evaluate frontal gap along the axis of the workpiece by the use of modified ECM theory, which takes into account effects of simultaneous variations in temperature, electrolyte conductivity, current density, and other related parameters. Bejar and Eterovich [6] examined wire-ECM for the cutting of mild steel with passivating electrolyte of $NaNO_3$. Wire-ECM has been studied by various researchers across the globe for optimizing its different process parameters.

Maeda et al. [7] studied the effect of processing parameters, such as electrolyte flow rate, nozzle diameter, and current density on the maximum feed rate of cutting during wire-ECM. Ningsong et al. [8] investigated wire-ECM with axial flushing of electrolyte for removing electrolysis products. They performed multi-wire electrochemical cutting. The side gap was kept within 200 μm. He et al. [9] established wire-ECM as a promising method for the fabrication of tungsten-based microstructure. With the help of pulsating DC power supply, they were able to restrict the side gap to 5 μm; feed rate used was 0.1 μm/s.

Xu et al. [10] used hydrophilic tungsten wire as cathode with a rough surface which was prepared by chemical etching. They found that by using a wire cathode with a rough surface, the machining stability improved, and the stable feed rate could be improved to 0.45 μm/s on cobalt base alloy with a thickness of 80 μm. Meng et al. [11] used wire-ECMM to machine Ni-based metallic glass. Several complex microstructures such as micro curved cantilever beam, micro gear, and micro square helix were successfully fabricated by them with different optimized parameters. Haidong et al. [12] proposed a method of wire-ECMM using axial vibration-assisted multi-wire electrodes with high traveling speed to improve the machining efficiency of wire-ECMM. They performed a series of experiments to optimize the parameters, and by using 15 wire electrodes, multiple slit microstructure of aspect ratio 20 is successfully fabricated by them with a very fine surface finish. Fang et al. [13] use large amplitude vibration of ribbed wire to enhance electrolyte renewal and bubble removal in wire electrochemical machining. Experimental results show that MRR and machining efficiency are greatly improved by using this method. Xiaolong et al. [14] propose a method using a rotary helical electrode to enhance electrolyte renewal in wire-ECMM. They simulated the rotary effect of helical electrode which helps electrolyte to generate an axial velocity that drags electrolyte from the bottom upwards. Experimental results show that when the electrolyte axial flow is accelerated by using a rotary helical electrode, the slit width uniformity in the depth direction is enhanced.

While working under the regime of micromachining each process parameter is to be carefully selected and maintained in order to obtain the desired output. The main problem associated with wire-ECMM is the side gap associated with it. In order to make this process suitable for micro machining, this side gap must be minimized to its lowest possible value. Fabrication of micro feature with the help of wire-ECMM is a challenging task mainly because of the side gap. Side gap cannot be fully eliminated, but it has to be reduced to the lowest possible value to achieve better machining accuracy. This side gap depends on different process parameters; type of electrolyte and its conductivity play a key role in ECMM. Conductivity of an electrolyte is dependent on its type, concentration as well as on temperature. Hence, it becomes necessary to choose their optimum value in order to achieve the best results. Another problem associated with any micromachining operation is its low MRR. Fabrication of micro features requires accuracy. For achieving this accuracy, most of the processes make a compromise with the MRR. The literature available on wire-ECMM revealed that some users use pulsed power supply which makes process a bit slow thereby reducing the MRR.

In the present work, an attempt is made to reduce the side gap in wire-ECMM for regulated DC power supply at a significantly high feed rate of 5 μm/s. The regulated DC supply and higher feed rate are used for achieving higher MRR to make this process more suitable for industrial applications. For this, in the first stage, three different workpiece materials, copper, aluminum, and stainless steel, are examined under identical conditions of the process parameters. Afterwards, effects of different electrolytes and their characteristics on the side gap of machined slits are analyzed. Electrolytes at elevated temperatures are also used to study the effect of electrolyte temperature on the side gap. Finally, with the help of commercially available copper wire of diameter 90 μm along with the optimum parameters obtained from different experiments, a slit with an average side gap of 26.8 μm is generated on a copper plate of thickness 200 μm.

2 Experimental setup

The schematic diagram of the experimental setup is given in Fig. 1.

The workpiece holder and electrolyte basin are mounted on X-Y drive, interfaced with computer using Arduino microcontroller. Regulated D.C. power supply with voltage rating from 0 to 32 V and minimum resolution for the current as 0.01 A is used. Electrolyte is delivered from the flexible delivery tube through a pressurized electrolyte tank. Maximum achievable flow velocity is 3 m/s. Wire is held tight in C-clamp. Copper, aluminum, and stainless steel workpiece of 200 μm thickness are used for the experiments. $NaNO_3$, NaCl, KCl, NaOH, HCl, $NaNO_3$ + HCl, NaCl + $NaNO_3$, NaOH + KCl that are used as electrolytes at constant concentration of 0.25 mol/L are used.

Figure 2 shows the schematic diagram of wire-ECM process. The characterizing parameters of a kerf like side gap (Δs) and frontal gap (Δb) are also labeled in this figure.

3 Results and discussion

In the first section, the current density distribution on the surface of workpiece and tool is obtained using Comsol Multiphysics software. The second section summarizes the results obtained for machining the slits with three different workpieces of aluminum, stainless steel, and copper. In the third section, copper as both tool and workpiece material,

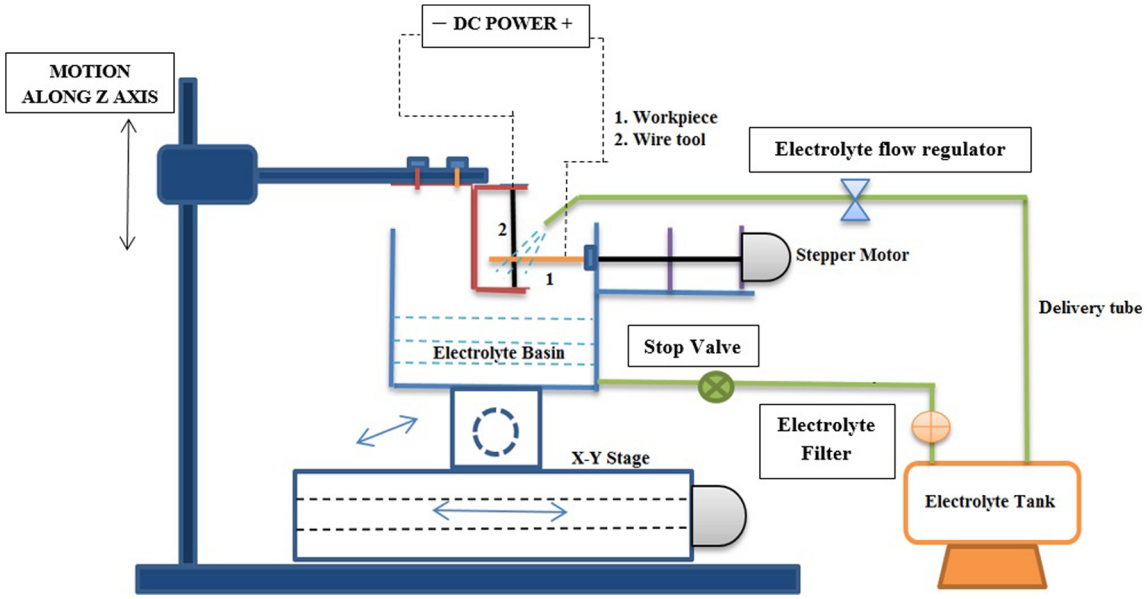

Fig. 1 Schematic diagram of wire-ECMM set-up

different electrolytes at a specific flow rate are analyzed. In the fourth section, electrolytes yielding minimum side gap in the third section are evaluated at varying temperatures, keeping other parameters constant. Finally, in the fifth section, most suitable parameters are selected for the fabrication of micro slits with the minimum side gap. At the end, average side gap of 26.80 μm is achieved on copper workpiece at a feed of 5 μm/s with the regulated D.C. power supply using KCl as electrolyte with a concentration of 0.25 mol/L at a pH of 7.6.

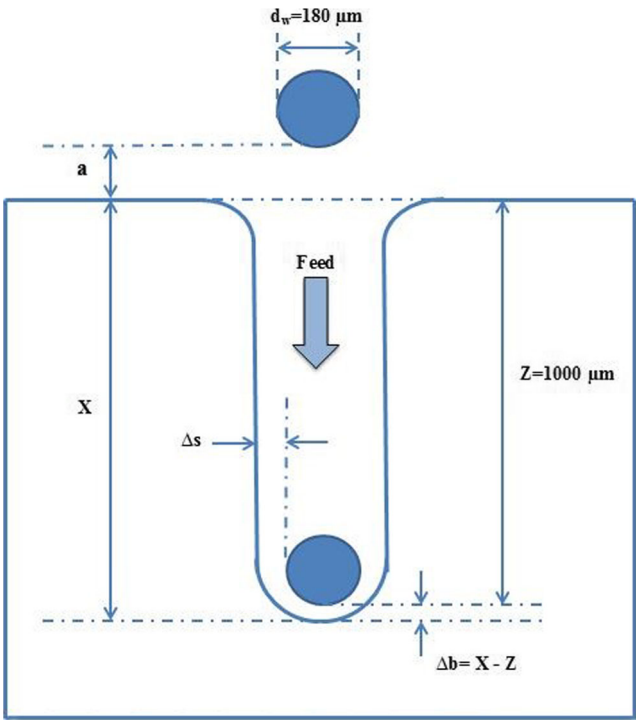

Fig. 2 Schematic of wire-ECMM process showing the wire insertion length and frontal gap

3.1 Current density distribution in wire-ECMM process

It can be seen from the simulation results that current density is relatively higher in the frontal gap as compared to that in side gap. The variation of current density in different regions between wire tool and workpiece anode is due to the variation of inter electrode gap in these regions. The lower the inter electrode gap, the smaller the resistance offered by the electrolyte in this region and higher the amount of current flowing through the path leading to rise in the local current density. Zhu et al. [15] showed that in case of wire-ECMM, the frontal gap is smaller than the side gap obtained. They expressed the relationship between these two parameters as follows:

$$\Delta_s \approx \Delta_b \sqrt{\frac{2d}{\Delta_b} + 1} \tag{1}$$

where Δ_b is the inter-electrode frontal gap, Δ_s is the machining side gap, and d is the wire diameter.

3.2 Side gap for different workpiece materials

While working with the regulated DC power supply and feed rate of 5 μm/s, Fig. 4 shows side gaps obtained for the slits on three different materials, namely, aluminum, copper, and stainless steel, while keeping all other parameters (electrolyte concentration, electrolyte flow rate, electrolyte temperature, feed rate of the workpiece, and the copper wire tool length) same. Side gap is measured at different locations and an overall average side gap is reported. The theoretical side gap is

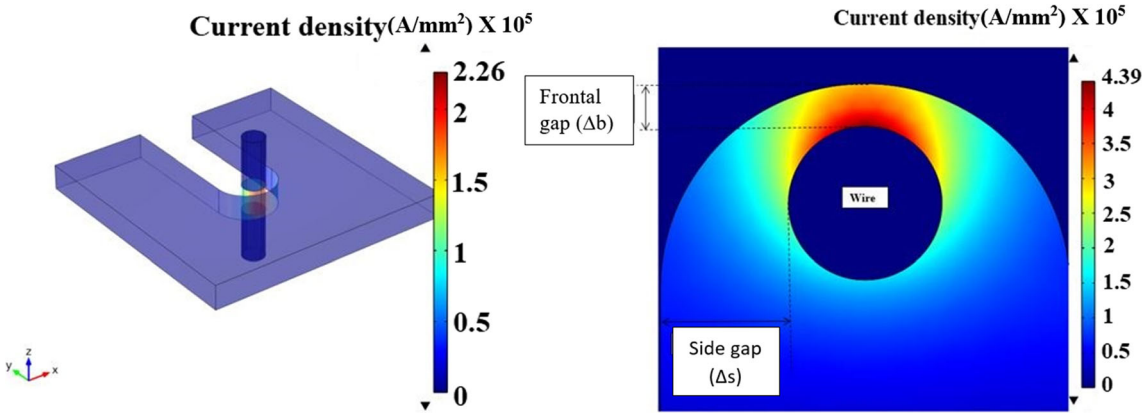

Fig. 3 Current density distribution in wire-ECMM in the regions around frontal gap and side gap

calculated using the expression in Eq. (1). Δb in the equation is the frontal inter electrode gap which is an equilibrium inter-electrode gap. This gap is obtained when the value of current flowing through the circuit becomes stationary. Assuming that the conductivity of electrolyte remains unaltered during the machining period, for a specific value of applied voltage, the value of current becomes constant when the inter electrode gap between the tool and workpiece becomes constant. Therefore, this value of constant inter electrode gap can be mathematically expressed as follows [16]:

$$\Delta b = \frac{\eta(V-\Delta V)k\,E}{F\rho f} \tag{2}$$

where η is the system current efficiency, V is the applied voltage in order to obtain constant current in the circuit, ΔV is the over-potential, k is the conductivity of electrolyte, E is the electrochemical equivalent of the workpiece material, ρ is the density of workpiece material, F is the faraday's constant, and f is the wire feed rate.

On substituting the value of frontal gap (Δb) from Eq. (2) into the expression for side gap in Eq. (1), the expression for side gap in terms of process parameters can be expressed as follows:

$$\Delta s \approx \left(\frac{\eta(V-\Delta V)kE}{F\rho f}\right)\left(\sqrt{\left(\frac{2d\rho Ff}{\eta(V-\Delta V)kE}+1\right)}\right) \tag{3}$$

The theoretical value of frontal inter electrode gap and then the value of side gap as shown in Figs. 3 and 4 is calculated for stationary current value of 0.15 A. The value of constant feed rate used for the experiments is 5 μm/s. Potassium chloride (0.25 mol/L) with electrical conductivity of 16.56 mS/cm is used as electrolyte. Diameter of wire (d) is 180 μm. For comparative study, the value of system current efficiency (η) is assumed as 1 and over potential (ΔV) is taken as zero. While machining copper at feed rate of 5 μm/s, the system assumes stationary current value of 0.15 A at potential of 16 V, while potential of 13 V in aluminum and 7.5 V for stainless steel served the purpose.

Machined slits are shown in Fig. 6. It can be clearly observed that minimum side gap was observed in the case of copper followed by stainless steel and aluminum.

Figures 4 and 5 clearly suggest that theoretical and experimental values for side gap and frontal gap for stainless steel and aluminum are in close agreement. But, there is a significant difference between these values for copper (Fig. 6).

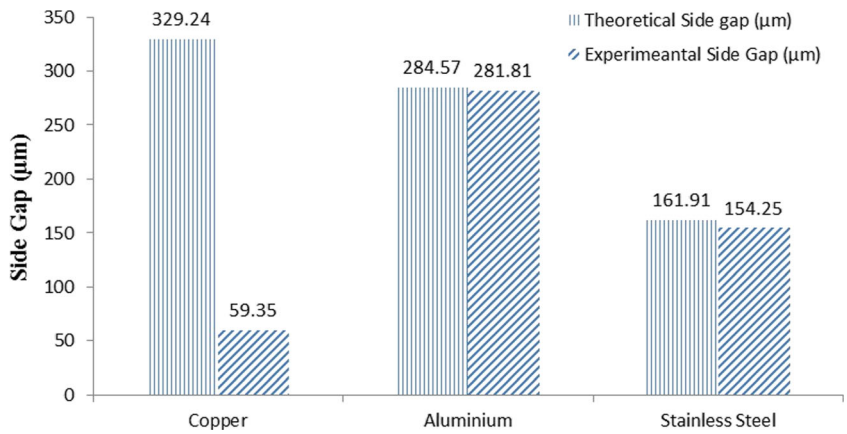

Fig. 4 Comparison between experimental and theoretical side gap for copper, aluminum, and stainless steel

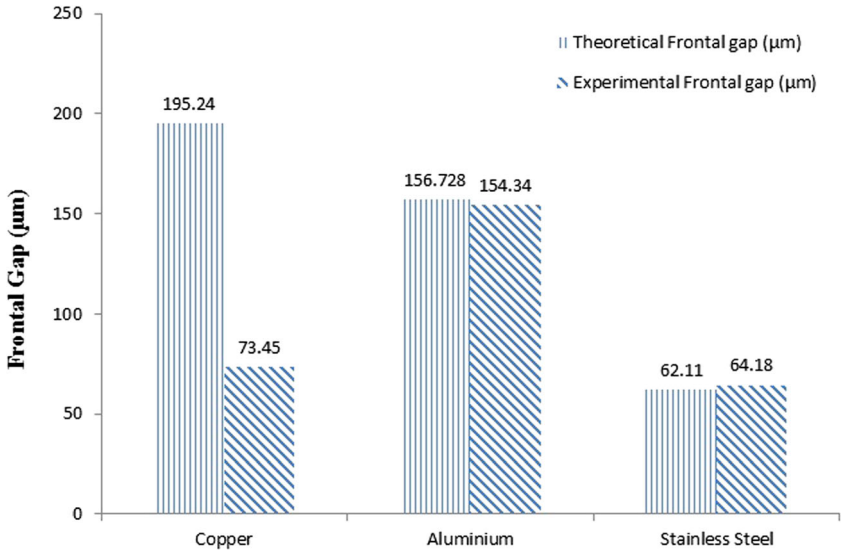

Fig. 5 Comparison between theoretical and experimental value of frontal gap for copper, aluminum, and stainless steel

3.3 Reason for discrepancy between the experimental and theoretical values for side gap and frontal gap in copper

The reason for the deviation between the experimental and theoretical values of side gap and frontal gap in case of copper is the formation of non-conducting passive layer on the surface of workpiece and acts as an extra resistance to the flow of current in the circuit.

$$I_{circuit} = \frac{(V - \Delta V)}{\left(R_{electrolyte} + R_{passive\ layer}\right)} \tag{4}$$

Figure 7 shows the presence of passive layer on the walls of kerf machined on copper.

This is one of the reasons why higher value of potential difference is required to obtain same value of constant current in the circuit for same electrolyte type and conductivity, wire feed rate, and workpiece thickness as compared with stainless steel and aluminum.

Figure 8 shows the pourbaix diagram for copper. The nature of dissolution of metal at a given value of electric potential and the pH value of electrolyte can be understood from a pourbaix diagram. The diagram clearly demarcates region of corrosion and passivation in terms of applied potential and pH value of electrolyte. The pH value of electrolyte used is 7.6, which is in the passivation zone leading to formation of copper oxide (CuO) as electrolysis products. This oxide is in the presence of external potential stick on the side wall of kerf (workpiece), although this layer is porous but highly non-conducting in nature and significantly reduces the rate of material removal from the workpiece surface.

The XRD imaging of the precipitate also confirms the presence of CuO in the sample. Figure 9 shows the XRD graph of the precipitate sample and standard XRD graph for CuO.

Linear material removal rate in ECM is given by the following:

$$MRR_l = \frac{(V - \Delta V)kE\eta}{F\rho y} \tag{5}$$

In case of passivation layer, a resistance offered by this layer modifies Eq. (5) and thus linear MRR in case of passivation can be written as follows:

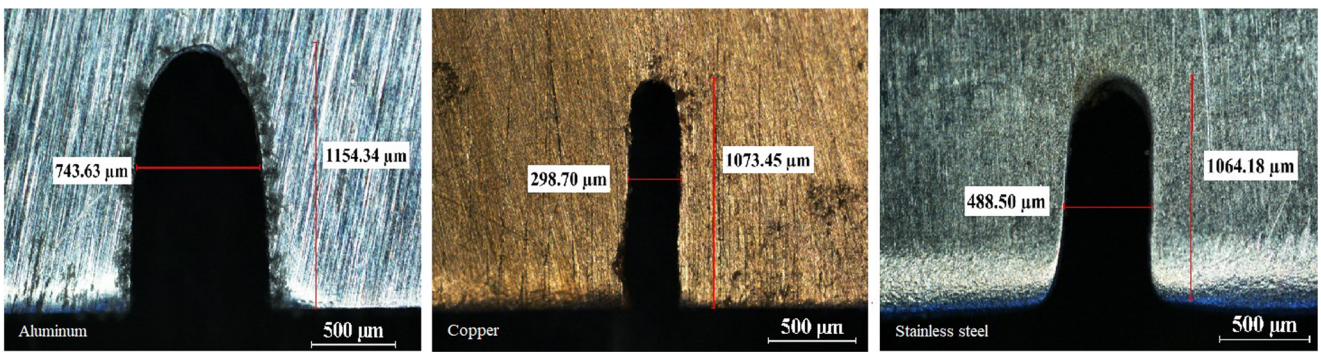

Fig. 6 Machined slits on aluminum, copper, and stainless steel

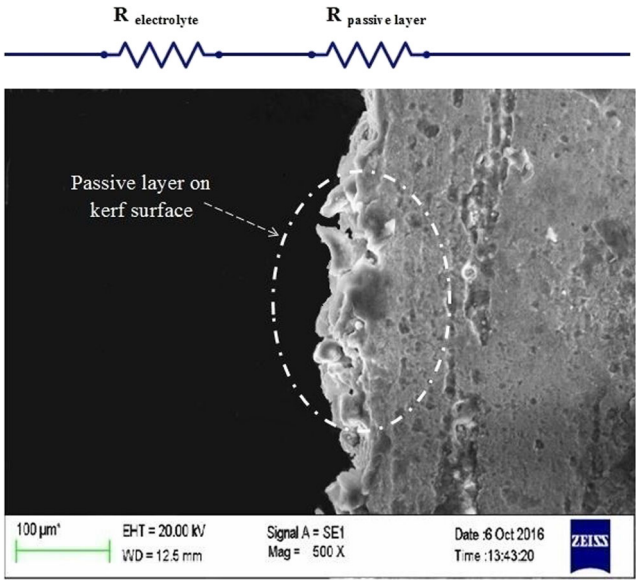

Fig. 7 Passive layer on the kerf wall in copper

$$MRR_l = \frac{(V-\Delta V)E\eta}{F\rho\left(\frac{y}{k}+R_P\right)} \tag{6}$$

where V is the applied voltage, ΔV is the over potential, E is the electrochemical equivalent of workpiece material, F is the faraday's constant, ρ is the density, y is the inter electrode gap, k is the conductivity of the electrolyte, and R_P is the resistance offered per unit area by the passivation layer and will vary according to the thickness of passivation layer that will vary essentially from point to point.

If f is feed rate given to the wire electrode, then the rate of change of linter electrode gap is given by the following:

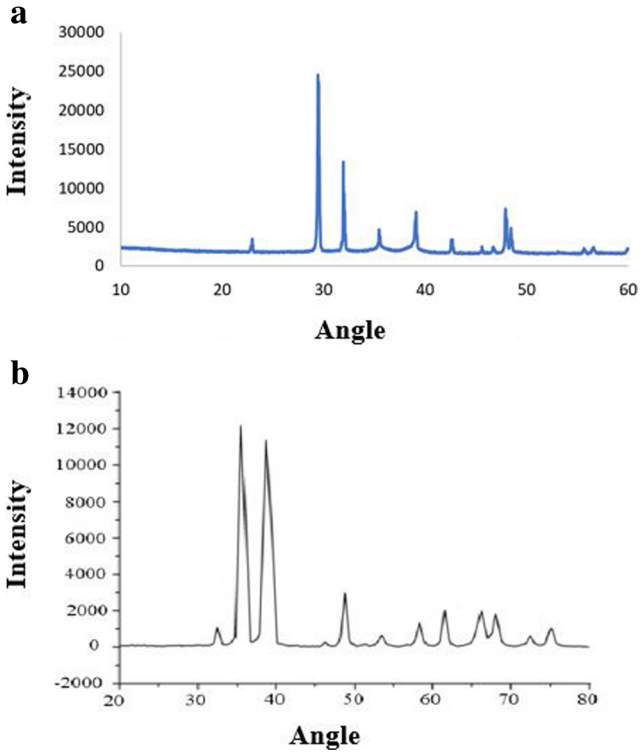

Fig. 9 **a** XRD graph of the precipitated sample. **b** Standard XRD graph of CuO for comparison

$$\frac{dy}{dt} = \frac{(V-\Delta V)E\eta}{F\rho\left(\frac{y}{k}+R_P\right)} - f \tag{7}$$

For stationary current to be constant, equilibrium IEG ($y_{eq.}$) should be maintained, i.e.,

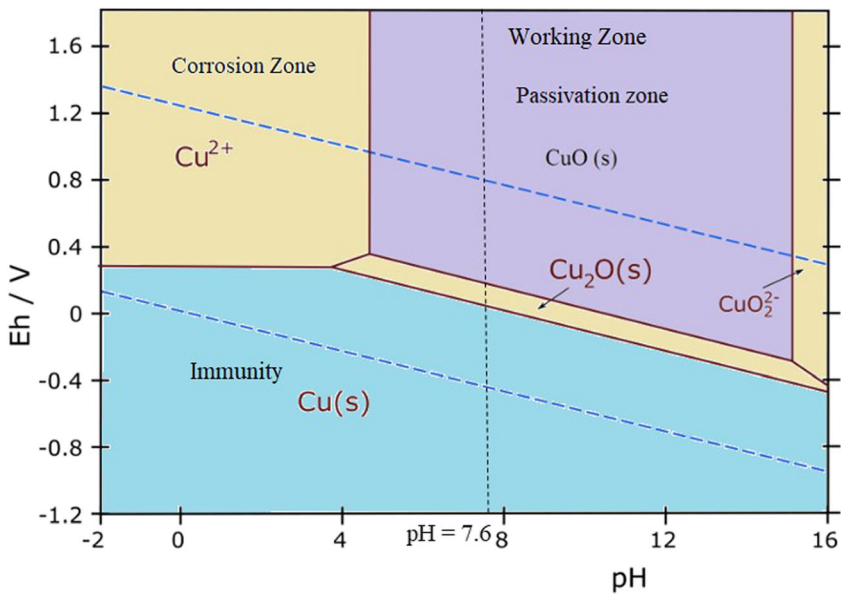

Fig. 8 Pourbaix diagram of copper indicating the working zone

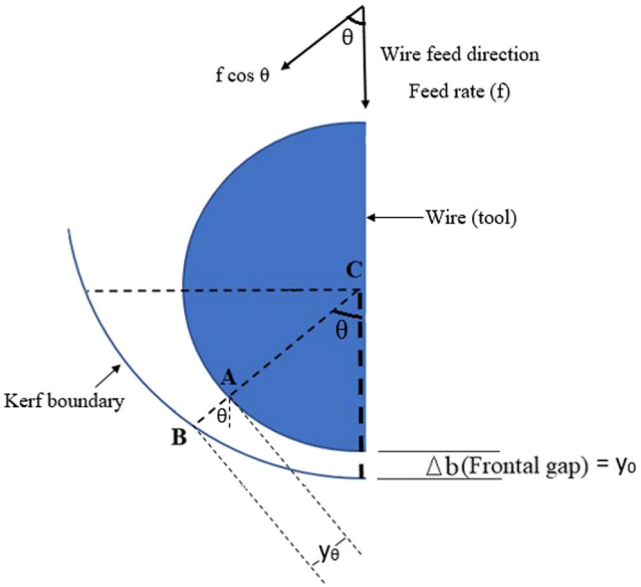

Fig. 10 Schematic diagram of wire-electrochemical slitting process showing the variation of IEG along wire periphery

$$\frac{dy}{dt} = 0f = \frac{(V-\Delta V)kE\eta}{F\rho\left(y_{eq.} + kR_P\right)} y_{eq.} + kR_P = \frac{(V-\Delta V)kE\eta}{F\rho f} y_{eq.} = \frac{(V-\Delta V)kE\eta}{F\rho f} - kR_P \tag{8}$$

Eq. 8 gives equilibrium IEG between the tool and the workpiece in case of passivation. In case of wire-ECM, this equilibrium IEG is the frontal gap of machining; thus, the frontal gap in case of passivation in W-ECM is given by the following:

$$\Delta b_P = \frac{(V-\Delta V)kE\eta}{F\rho f} - kR_P \tag{9}$$

When there is no passivation, the frontal gap is given by the following:

$$\Delta b = \frac{(V-\Delta V)kE\eta}{F\rho f} \tag{10}$$

Thus Eq. (10) can be written as follows:

$$\Delta b_P = \Delta b - kR_P \tag{11}$$

where (Δb_p) is the frontal gap in case of passivation and (Δb) is the frontal gap in case of no passivation. R_p in the above equation is not a constant value and will vary along the length of the kerf. The value of R_p will depend upon the thickness of passivation layer which will essentially be different at different points.

The IEG is varying continuously along the boundary of the kerf. Figure 10 shows the schematic diagram of the process.

The rate of change of IEG at any angle "θ" to the feed direction in case of passivation can be written as follows:

$$\frac{dy(\theta)}{dt} = \frac{(V-\Delta V)E\eta}{F\rho\left(\frac{y_\theta}{k} + R_{P\theta}\right)} - f\cos\theta \tag{12}$$

For stationary current to be constant, equilibrium IEG ($y_{eq.(\theta)}$) can be expressed as follows:

$$f\cos\theta = \frac{(V-\Delta V)kE\eta}{F\rho\left(y_{eq.(\theta)} + kR_{P\theta}\right)} \tag{13}$$

$$y_{eq.\theta} = \frac{(V-\Delta V)kE\eta}{F\rho f\cos\theta} - kR_{P\theta}\left(\text{For } 0^0 < \theta < 90^0\right) \tag{14}$$

where $R_{p\theta}$ is the resistance due to passivation layer at any angle θ.

3.4 Side gap for different electrolytes

Equimolar concentration of different electrolytes is examined under the identical conditions of process parameters. In order to make significant study, electrolytes with basic, acidic, and near neutral nature are analyzed for side gap. Main motivation for this study is the fact that electrolysis products at the tool and workpiece behave differently in different electrolytic medium. Few electrolyte mixtures were also prepared and employed for cutting slits on copper workpiece.

Other process parameters chosen for this purpose are as follows: electrolyte concentration = 0.25 mol/L, feed rate = 5 μm/s, and electrolyte flow rate = 2 m/s, which is set by varying volume flow rate of electrolyte from a fixed cross-sectional area (Table 1).

The voltage is chosen such that the desired feed of 5 μm/s can be achived in each case without any short circuit or undulation. The potential required for machining at the feed rate of 5 μm/s when KCl, NaCl, and NaOH are used as electrolytes is high. It is due to this reason that these three electrolytes are analyzed for a higher value of electric potential (15 V), while

Table 1 Electrolytes and corresponding average side gap

S.No.	Electrolyte	Voltage (V)	Side gap (μm)
1	$NaNO_3$	7	368.980
2	HC1	7	373.510
3	NaC1 + $NaNO_3$	7	432.129
4	NaOH + KC1	7	190.185
5	$NaNO_3$ + HC1	7	505.926
1	KC1	15	55.450
2	NaOH	15	118.889
3	NaCI	15	58.23

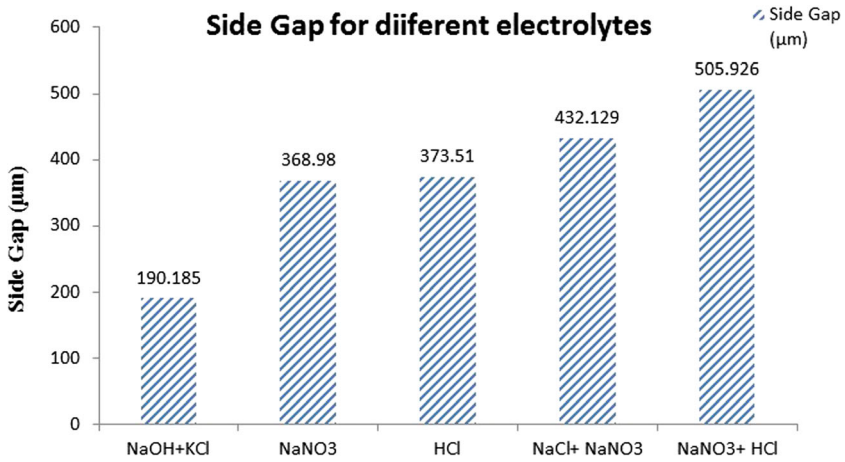

Fig. 11 Side gap obtained for different electrolytes at a feed rate of 5 μm/s

other electrolytes are analyzed for a lower value of electric potential (7 V). From the above analysis, a significant observation is derived that even when electric potential in last three cases is high, the average value of side gap is much lower as compared to other electrolytes. This is because side gap is dependent on the combined effect of electrolyte conductivity and the passivation layer formed due to the reaction products forming while machining. In this investigation, KCl gives the better result in terms of side gap. The highest side gap was obtained for HCl in individual case of electrolytes, while in over all, the highest value of side gap was achieved in case of $NaNO_3$ + HCl.

3.5 Side gap for different electrolytes at varying temperature

From the results of previous experiments (Figs. 10 and 11), minimum side gap is obtained for KCl (55.45 μm), followed by NaCl (58.23 μm) and NaOH (118.889 μm). The best three electrolytes were selected for evluating the effect of electrolyte temperature on the side gap obtained. While working with NaOH and its mixture with KCl, the problem of excessive sludge formation and undulations in the slit occurred. Therefore, instead of NaOH and its mixture, the next best electrolyte, which is $NaNO_3$, is used for the analysis. Slits were examined for four different temperatures 30, 45, 55, and 65 °C (Fig. 12).

In general, the MRR while working with $NaNO_3$ is lower as compared to MRR obtained when working with KCl and NaCl. However, for machining copper with passivating electrolyte like KCl and NaCl passivation alters the rate of material removal significantly (Fig. 8) and material removal is lowered. The same trend is reflected in average side gap as shown in Fig. 13.

From the above experiments, it is evident that low temperatures are favorable for fabricating finer slits. This result can be understood by the conductivity factor of electrolyte. It is a well known fact that conductivity of electrolyte increases with rise in temperature, which leads to higher MRR at higher temperature. This results in increase in side gap at higher temperatures. However, electrolyte conductivity is also governed by void fraction and sludge formation. Jain and Chouksey [17] showed that electrolyte electrical conductivity during electrochemical machining varies due to generation of gas bubbles at the tool and workpiece surfaces, sludge due to the dissolution of workpiece material, and heat due to flow of electric current in the circuit. This makes the electrolyte to

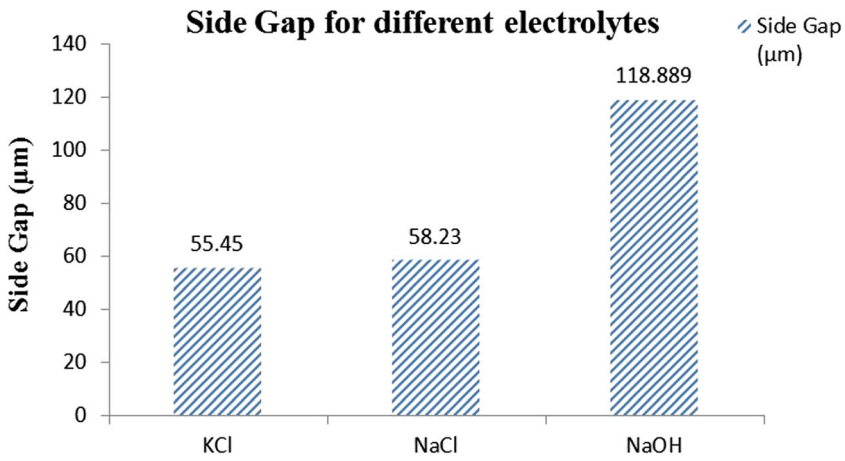

Fig. 12 Side gap for different electrolytes at feed rate of 5 μm/s for copper

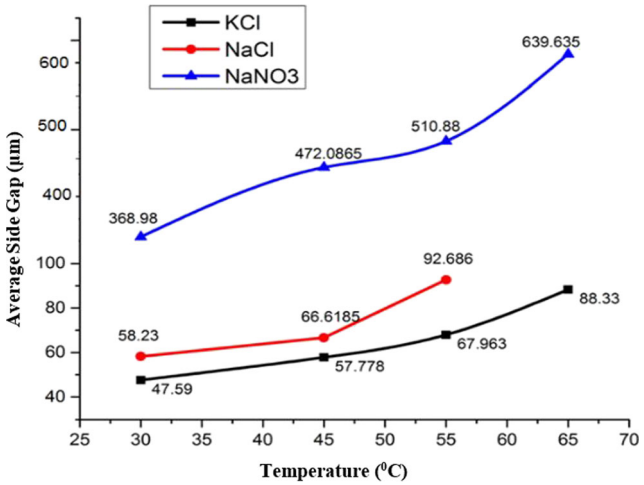

Fig. 13 Side gaps obtained for different electrolyte at varying temperatures

behave as a multiphase system. It was reported that if IEG is very small (less than 200 μm), the electrolyte conductivity reduces by more than 20% at a potential of 10 V; hence, at small IEGs, the effect of bubble and sludge seems to dominate the effect of heat generation, leading to net reduction in electrolyte electrical conductivity. The effective electrolyte electrical conductivity is given by the expression:

$$k_{eff} = \frac{k_0 D_{int}}{H}\left\{1 + \frac{E^2 k_0 \eta}{\rho_e u\, \delta^2 C_e} D_{int}\right\}$$

where k_{eff} is the effective conductivity, k_0 is the initial electrical conductivity of continuos medium, H is the length of workpiece along the electrolyte flow direction, E is the applied potential across the electrodes, is the temperature coefficient of specific conductance, 휂 is the IEG, C_e specific heat capacity of electrolyte, u is the velocity of elctrolyte between electrodes, ρ_e is the density of electrode material. However, in the present study, electrolyte is considered as a single phase medium and its dependency on void fraction and sludge formation is neglected. Patel et al. [18] successfully generated micro textures on metallic surfaces like micro dimple array, micro channels and micro pillars by carefully selecting the optimal machining conditions for micro feature generation using electrochemical micro machining.

Table 2 Parameters used for making micro-slit

Parameters	Specifications
Workpiece	Copper
Electrolyte	KC1
Concentration of electrolyte	0.25 mol/L
Flow rate of electrolyte	2 m/s
Feed rate	5 μm/s
Voltage	14 V DC
Temperature	26 °C

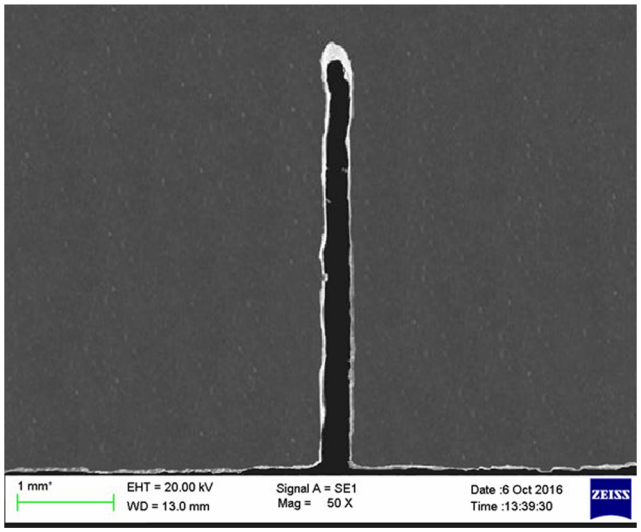

Fig. 14 Micro slit of average side gap = 26.8 μm machined on copper (machining conditions in Table 2)

Other significant observation that was derived from this experiment is that undulations on slit increased with temperature rise. In case of NaCl while machining at temperature of 65 °C, undualtaions were high that machining was nearly impossible. This accounts for the missing point in the above graph while machining with NaCl.

3.6 Fabrication of microslit on copper

Results obtained from previous experiments are utilized for the fabrication of microslit. These conditions are summarized in the Table 2.

Using this wire as a tool (diameter is 90 μm) and above mentioned input parameters, a slit with a minimum side gap of 24.4 μm and maximum side gap of 29.2 μm had been machined succesfully. The wire is inserted to a depth of 2750 μm. It is important to note that feed employed from the fabrication of the feature is well beyond the recommended feed for micromachining. Hence, these parameters can be utilized for performing micromachining operations at rapid speeds (Fig. 14).

4 Conclusion

1. The pH of the electrolyte solution and working potential are the deciding factors which determines the nature of anodic dissolution. Higher material removal rate can be obtained when electrolyte pH and working potential promote corrosion. Higher surface finish can be obtained when passivation phenomenon is dominant.

2. The use of KCl (pH > 7) for machining copper generally leads to passivation of the anodic surface and large dissimilarity is observed between the theoretical and experimental values of side gap and frontal gap.
3. Experimental observations show that in order to obtain higher values of MRR for a given value of applied potential, electrolytes at elevated temperatures must be used. This is due to rise in electrolyte electrical conductivity at increased temperature leading to increase in MRR. However, it is true only up to a certain temperature.
4. Among the eight different electrolytes used for machining of copper, KCl is observed to have a highest degree of passivation and the minimum side gap is achieved in this case. The use of KCl promotes the formation of CuO as an electrolysis product which later gets deposited on the walls of the kerf and reduces the overall conductivity of the passage.
5. Finally, an average side gap of 26.8 μm is successfully achieved with the help of an in situ fabricated wire and at the optimum conditions which are found out experimentally, at a significant feed of 5 μm/s using regulated DC power supply.

Acknowledgements Authors acknowledge the help of Manufacturing Science lab at I.I.T Kanpur for providing necessary conditions required to perform the above experiments.

References

1. Jain VK, Rajurkar KP (1991) An integrated approach for tool design in ECM. Precis Eng 13(2):111–124
2. Bhattacharyya BDPSB, Doloi B, Sridhar PS (2001) Electrochemical micro-machining: new possibilities for micro-manufacturing. J Mater Process Technol 113(1):301–305
3. Munda J, Bhattacharyya B (2008) Investigation into electrochemical micromachining (EMM) through response surface methodology based approach. Int J Adv Manuf Technol 35(7):821–832
4. da Silva Neto JC, da Silva EM, da Silva MB (2006) Intervening variables in electrochemical machining. J Mater Process Technol 179(1):92–96
5. Jain VK, Pandey PC (1980) An analysis of electrochemical wire cutting process using finite element technique. Proceeding of 20th MTDR Conference pp 631–636
6. Bejar MA, Eterovich F (1995) Wire-electrochemical cutting with a NaNO3 electrolyte. J Mater Process Technol 55(3–4):417–420
7. Maeda R, Chikamori K, Yamamoto H (1984) Feed rate of wire electrochemical machining using pulsed current. Precis Eng 6(4): 193–199
8. Qu N, Fang X, Li W, Zeng Y, Zhu D (2013) Wire electrochemical machining with axial electrolyte flushing for titanium alloy. Chin J Aeronaut 26(1):224–229
9. He H, Zeng Y, Qu N (2016) An investigation into wire electrochemical micro machining of pure tungsten. Precis Eng 45:285–291
10. Xu K, Zeng Y, Li P, Fang X, Zhu D (2016) Effect of wire cathode surface hydrophilia when using a travelling wire in wire electrochemical micro machining. J Mater Process Technol 235:68–74
11. Meng L, Zeng Y, Zhu D (2017) Investigation on Wire Electrochemical Micro Machining of Ni-based Metallic Glass. Electrochim Acta 233:274–283
12. He H, Zeng Y, Yao Y, Qu N (2017) Improving machining efficiency in wire electrochemical micromachining of array microstructures using axial vibration-assisted multi-wire electrodes. J Manuf Process 25:452–460
13. Fang XL, Zou XH, Chen M, Zhu D (2017) Study on wire electrochemical machining assisted with large-amplitude vibrations of ribbed wire electrodes. CIRP Ann Manuf Technol 66:205–208
14. Xiaolong F, Pengfei Z, Yongbin Z, Ningsong Q, Di Z (2016) Enhancement of performance of wire electrochemical micromachining using a rotary helical electrode. J Mater Process Technol 227:129–137
15. Zhu D, Wang K, Qu NS (2007) Micro wire electrochemical cutting by using in situ fabricated wire electrode. CIRP Ann Manuf Technol 56(1):241–244
16. Jain VK (2002) Advanced machining processes, electrochemical machining (ECM). Allied publisher, New Delhi, pp 232–279
17. Jain VK, Chouksey AK (2017) A comprehensive analysis of three-phase electrolyte conductivity during electrochemical macromachining/micromachining. Proc Inst Mech Eng, Part B: J Eng Manuf 1–13. https://doi.org/10.1177/0954405417690558
18. Patel D, Jain VK, Ramkumar J (2016) Micro texturing on metallic surfaces: State of the art. Proc Inst Mech Eng, Part B: J Eng Manuf. https://doi.org/10.1177/0954405416661583